



Effect of Ni doping on the microstructure and magnetic properties of Fe–Ga ribbons

H. Liu¹ · Z. Z. Zhang¹ · Y. J. Wu² · L. M. Dong³ · H. O. Wang⁴ · M. X. Cao⁵ · W. S. Tan⁶

Received: 24 July 2019 / Accepted: 18 September 2019 / Published online: 24 September 2019
© Springer Science+Business Media, LLC, part of Springer Nature 2019

Abstract

A set of Ni doping Fe–Ga ribbons were fabricated using melt spinning method. The microstructure was studied using extended X-ray absorption fine structure spectroscopy (EXAFS), high resolution X-ray diffraction (HRXRD) and metallurgical microscope. The results of microstructure indicated that as Ni concentration increased, the lattice matrix transformed from body-centred cubic (bcc) to face-centred cubic (fcc), with the decrease of unit cell volume and the emergence of little amount B₂ and E₂₁ phase. The result of magnetic and magnetostrictive properties showed that the saturation magnetization decreased with Ni doping. (110) texture in studied ribbons resulted in low saturation magnetic field and high saturation magnetostriction. In addition, small amount of precipitated phase E₂₁ improved the magnetostriction of FeNiGa ribbons.

1 Introduction

In recent years, it has been found that doping Ga into pure Fe can effectively improve its magnetostrictive properties [1]. Compared with the traditional magnetostrictive material TbDyFe which is of intrinsic brittleness, Fe–Ga alloy has many advantages, such as low cost, good ductility and so on. Therefore, it has become a good substitute for TbDyFe. Researchers have revealed that the magnetostriction of Fe–Ga alloys relied not only on Ga composition, but also on fabrication technology and heat treatment method

since these factors produced different texture and grain morphologies [2–6]. Until now, it is commonly believed that the modified-DO₃ phase plays a key role in increasing the magnetostrictive coefficient of Fe–Ga alloy [7–9]. In modified-DO₃ phase, the next-nearest-neighbor pairs of Ga atoms along the direction of [100] can reduce the elastic modulus and increase the magnetoelastic coupling, thus improving the magnetostrictive properties of Fe–Ga alloys [10]. In addition, (100) texture resulted from certain fabrication technology is also considered to improve the magnetostrictive properties of Fe–Ga alloys [11]. However, the magnetostriction of Fe–Ga alloy is still too small comparing with that of TbDyFe alloys [12]. This shortcoming will limit its application.

Lately, special attentions have been paid to the effects of doping small amounts of third elements into Fe–Ga alloy in order to obtain larger magnetostriction. The doped elements mainly include rare earth, transition metal and so on. The results on rare earth elements doping indicates that small amount of Tb and Dy increase the magnetostriction of Fe–Ga based alloy about 2–3 times due to strong localized magnetocrystalline anisotropy of Tb and Dy elements [13, 14]. Moreover, the light rare earths like Ce and Pr can soften the tetragonal modulus via their crystal field interaction and then improve the magnetostriction [15]. In Sm-doped samples, the stronger local magnetocrystalline anisotropy causes larger enhancement in magnetostrictions. [16].

Although rare earth doping can effectively improve the magnetostrictive properties of Fe–Ga alloys, the brittleness

✉ H. Liu
hyitliuh@163.com

W. S. Tan
tws03221005@126.com

¹ Faculty of Applied Technology, Huaiyin Institute of Technology, Huaian 223001, China

² Department of Materials Science, Institute of Molecular Materials and Devices, Fudan University, Shanghai 200438, China

³ School of Automotive Engineering, Changshu Institute of Technology, Changshu 215500, China

⁴ Institute of Materials Physics, Hangzhou Dianzi University, Hangzhou 310018, China

⁵ College of Chemistry and Molecular Engineering, Peking University, Beijing 100871, China

⁶ College of Communication and Electronic Engineering, Hunan City University, Yiyang 413002, China

of the materials increases with rare earth doping. In addition, considering the high price of rare earth, other doping elements which can improve the magnetostrictive properties while ensuring the toughness of materials need to be found urgently. As a flexible metal, proper addition of Al can improve the tensile ductility, but the magnetostrictive properties is deteriorated [17]. Of particular concern is the doping of transition elements because the addition of transition metals like V, Cr, Mo does not change the toughness of materials and increase the magnetostriction of pure iron [18]. Therefore, doping of transition metals may solve the current predicament of Fe–Ga alloys. Previous studies have shown that the influence factor of transition metal doping on magnetostrictive properties of Fe–Ga alloys has not yet been determined and there seems to be a paradox in the results. For example, doping of 2 at.% of 3d and 4d transition elements such as Mn and Co reduces the magnetostriction of Fe–Ga single crystal because 3d transition elements stabilize the DO_3 structure, which decrease the magnetostriction [19–21]. But results in Refs. [22, 23]. indicate that the substitution of Mn(0–16 at.%) and Co(0–10 at.%) for Fe enhance the magnetostriction of Fe–Ga polycrystalline slightly. When small amounts of Ni are doped in Fe–Ga single crystal, the magnetostriction decrease [24]. Similar to the case of Co addition, the decrease of magnetostriction is believed to be resulted from DO_3 phase which is stabilized by the addition of transition elements. But adding small amounts of Ni in Fe–Ga melt-spun ribbons plays a positive role in the magnetostriction [11]. Bormio-nunes et al. believes [11] that the enhanced magnetostriction is attributed to the strong (100) texture and additional DO_3 phase, but even though in (100) single crystal from Ref. [24], the magnetostriction do not increase with the stronger (100) texture and additional DO_3 phase. These inconsistent results indicate that (100) texture and DO_3 phase may not be the key factors influencing magnetostriction in Ni-doped ternary Fe–Ga alloys. Therefore, it is essential to study the factor influencing the magnetostriction of FeNiGa alloys and guild researcher to get larger magnetostriction in Fe–Ga-based alloys. At the same time, the results on Ni-doped ternary Fe–Ga alloys will be helpful for researcher to elucidate the origin of magnetostriction in binary Fe–Ga alloys and ternary alloys doped with other transition elements. From the discussion above, it is believed that there are many rich physical images in the field of transition metal doping. In the process of sample preparation, preparing method will influence the magnetostriction of Fe–Ga based alloys by forming texture in the sample. As a convenient and effective fabrication technology, melt-spinning method would promote the formation of texture in samples by means of temperature gradient and then enhance the magnetostriction of both binary and ternary Fe–Ga alloys, so this preparing method was chosen in this study.

To determine the key factors affecting the magnetostrictive properties of Ni-doped Fe–Ga ternary alloys, here, we present an experimental study that aims at investigating the crystallographic, microstructural, magnetic and magnetostrictive properties of a series of Ni-doped polycrystalline ribbons of composition, $Fe_{81-x}Ni_xGa_{19}$ ($0 \leq x \leq 25$). In particular, to detect the splitting of the diffraction peaks which are difficult to distinguish because of the close scattering factors between Fe and Ga atoms, HRXRD in synchrotron facility was used in this work. Results obtained in this research effort represent an exceptional increase in the magnetostriction coefficient of [110]-textured Fe–Ga alloys. This is contrary to the previous (100) texture promoting magnetostrictive properties of Fe–Ga alloys. The optimal composition for the best magnetostrictive response is found to be the sample of $x = 15$. Besides, a previously unreported $E2_1$ phase was observed in our samples by HRXRD. At last, the origin of the enhanced magnetostrictive effect in this materials system is discussed in the context of the microstructure. Overall, this work deepens the understanding of magnetostriction of the third element doped Fe–Ga alloy and has guiding significance for finding new magnetic materials with giant magnetostrictive properties.

2 Experiment details

Before the ingots were prepared, high purity (99.99%) Fe, Ga and Ni were cut into small pieces and weighed according to the chemical ratio. Subsequently, the ingots of FeNiGa alloy were prepared by arc-melting Fe, Ga and Ni four times, and then homogenized at 1273 K for 8 h under argon atmosphere. Ribbons with a thickness of ~ 30 – $70 \mu\text{m}$ were prepared by single roller melt spun method. HRXRD patterns were measured at beam line BL14B at Shanghai Synchrotron Radiation Facility (SSRF) with wavelength of 0.12438 nm and energy resolution of 4.4×10^{-4} . The transmission Ga K-edge EXAFS of studied ribbons were investigated using double crystal Si (111) monochromator at beam line BL14 W of SSRF. The ribbons were polished to be about $30 \mu\text{m}$ thickness to provide a unit absorption jump at the GaK-edge. The cross-sectional micrographs of the ribbons were obtained by optical microscope (Zeiss). The process is as follows: The samples embedded in the cold inlay were polished on sandpaper together with the cold inlay. The order of sandpaper selection is from 400 to 1000 mesh. The polished samples were placed on the polishing machine for mechanical polishing until a bright mirror was seen in the microscope. After being corroded by chemical solution, the micrographs were observed. The metallographic samples were prepared though cold setting, polishing in proper order and etching in corrosive liquid. The stacked samples were made by gluing about 20 ribbons together, then the

standard strain gauges were stuck on the surface of stacked samples. To measure the magnetostriction, the magnetic field was applied along the normal direction of the ribbon plane. Magnetization of ribbons was measured by the vibrating sample magnetometer (VSM) system (Lakeshore 7400 Series). In measurement, the magnetic field is parallel to the length direction of the ribbons.

3 Results and discussion

HRXRD spectra of FeNiGa thin ribbons is shown in Fig. 1a. It can be seen from the figure that there are obvious (110), (200) and (211) diffraction peaks in each XRD spectrum, which are characteristic peaks of the disordered alpha-Fe phase (A2 phase). The characteristic peaks of L1₂ phase are observed from HRXRD when $x \geq 15$. The details of the diffraction spectrum of $x = 15$ and 20 are shown in Fig. 1b. The splitting of (110) peak of A2 phase and the shoulder peak of (200) plane of L1₂ phase are found in the sample of $x = 15$, and a superlattice diffraction peak is found at 24.7°. The splitting of A2 phase (110) diffraction peak and the superlattice diffraction peak at 24.7° indicates that a new body centered cubic (bcc) phase appears in the sample. In Fe–Ga alloys, the ordered bcc phase is DO₃ phase or B2 phase. If the new bcc phase is DO₃ phase, the peak (1/2, 1/2, 1/2) which belongs to DO₃ phase can be observed more easily besides the diffraction peak at 24.7°. However, there are no (1/2, 1/2, 1/2) peaks in Fig. 1b, so it can be determined that the new bcc phase appearing in $x = 15$ sample is B2 phase. The phase diagrams of FeNiGa ternary alloys also support this result from another aspect [25]. The shoulder peak of the L1₂ (200) diffraction peak in the face-centered cube (fcc) is due to the appearance of E2₁ phase [26]. For the $x = 20$ sample, a weak shoulder peak appears on the left side of the A2 (211) diffraction peak, as shown in Fig. 1b. Similar to $x = 15$, this shoulder peak also indicates the existence of B2 phase [25]. Only A2 and L1₂ phases are observed in $x = 25$ samples. The diffraction index of each diffraction peak is shown in Fig. 1.

The cross-sectional micrographs of our ribbons are shown in Fig. 2. All the ribbons display columnar grains in the solidification direction. The formation of columnar grains originates from large temperature gradient along the normal direction of ribbon during quenching procedure. From Fig. 2 we conclude that the grain size increase with increasing of Ni concentration in FeNiGa ribbon. This result is in agreement with that of HRXRD because larger peak width of FeNiGa ribbon in HRXRD patterns usually represents smaller grain according to Scherer's formula. In micrograph images of ribbons with $x = 15$ and $x = 20$, some dark dotlike phase precipitate. The dotlike phase almost disappear and large contrast between grains in the image is detected

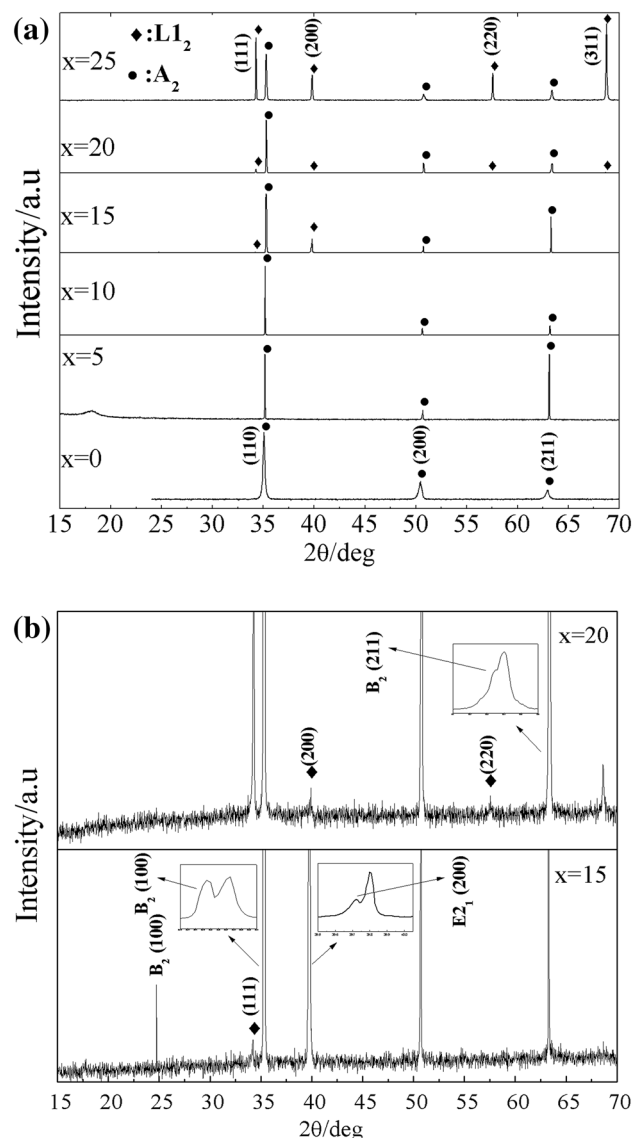


Fig. 1 a HRXRD patterns of FeNiGa. b The magnified HRXRD patterns of ribbons for $x = 15$ and $x = 20$. Insets show the splits of diffraction peaks in detail

for FeNiGa ribbon with $x = 25$. Referring to the result of HRXRD shown in Fig. 1 and the phase diagram of FeNiGa alloys [25], we believe that these dotlike phase probably is E2₁ phase or B2 phase which contained more Ga atoms comparing with disordered A2 phase, whereas large contrast between grains in the image of ribbon with $x = 25$ is related to large amount of L1₂ phase.

Table 1 shows the structure parameters calculated from HRXRD spectra. When the content of Ni increases from 0 to 25 at. %, the lattice constant a of A2 phase decreases from 0.29193 to 0.29002 nm. Compared with the standard diffraction patterns of Fe polycrystalline powder, the samples $x = 5$ and $x = 15$ exhibit strong (211) texture. When Ni element is

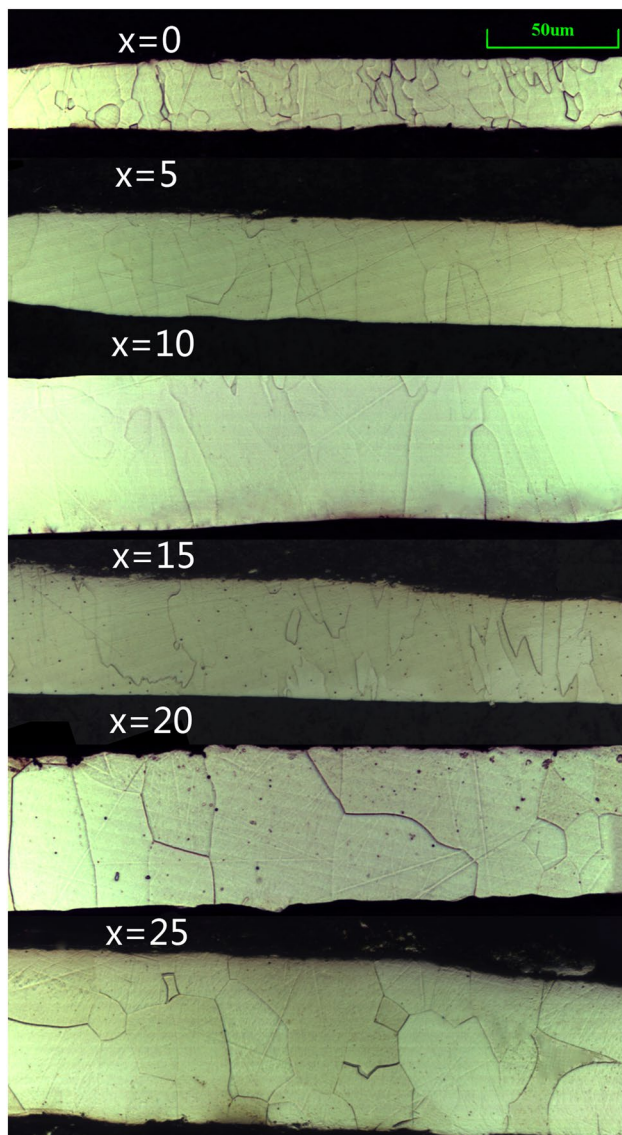


Fig. 2 Micrograph of the ribbons melt-spun at velocity of 7 m/s

doped into Fe–Ga alloy, the ratio of I_{200}/I_{110} is obviously smaller than that of $Fe_{81}Ga_{19}$ ribbon. With the increasing of Ni content, the ratio of I_{200}/I_{110} first decreases and then increases, and reaches its maximum at $x = 10$. We believe

that the substitution of Ni for Fe results in (110) texture in the sample. As can be seen from the data in Table 1, no (100) texture is found in the FeNiGa ribbon.

HRXRD was only sensitive to the long-range ordering (LRO) but could not be used to detect the local structure of materials. In order to study the local structure of FeNiGa ribbons, GaK-edge EXAFS of all the ribbons were measured in SSRF. More experimental details are given in Ref. [27], [28]. Figure 3a shows the EXAFS of FeNiGa ribbons, from which we find that the absorption jump at GaK-edge of all the studied ribbons are in the range from 1 to 2. This ideal absorption jump results in good signal-to-noise ratio and make our analysis more reliable. For the EXAFS analysis, we used the following conventional procedure: background removal, base-lining of oscillation, determination of absorption edge energy, normalization of spectral intensity by edge jump, and then Fourier transformation, therefore the radial distribution function (RDF) would be obtained [29]. In this procedure, the pre-edge background was subtracted with a linear function while R_{bkg} parameter was equal to 0.12 nm. The k^2 weighted $\chi(k)$ data, to enhance the oscillations at higher k , were Fourier transformed (FT) which was calculated using the Hanning filtering function. As shown in Fig. 3b, the RDF has an intense peak at an interatomic distance of about 0.22 nm, which corresponds to the nearest neighbor (NN) interatomic pair around Ga atoms; the subsidiary peaks correspond to 2nd, 3rd, and 4th NN interatomic pairs. As the Ni concentration x increase from $x = 0$ to $x = 20$, there is no obvious shape change in RDF but the position of second peak moves left slightly. We know that in RDF the position of peaks is related to the coordination distance. The decrease of coordination distance is in accord with the result of lattice constant obtained from HRXRD pattern. When the Ni concentration increased to $x = 25$, the RDF varied sharply, especially in the range from 0.3 to 0.5 nm, which was marked with black lines in Fig. 3b. This obvious change in RDF should result from a remarkable bcc–fcc transform. The fitting of EXAFS data was not performed here because too many elements would make the fitting results unreliable.

From above analysis we can summarize the structure of studied ribbons as follows. The ribbons with Ni

Table 1 Lattice constant, ratio of intensity of diffraction peak, saturated magnetization, saturated magnetic field and saturated magnetostrictive coefficient of the ribbons

| Composition x | A (nm) | I_{211}/I_{110} (%) | I_{200}/I_{110} (%) | M_s (emu/g) | H_s (kA/m) | λ_s (ppm) |
|---------------------|----------|-----------------------|-----------------------|---------------|--------------|-------------------|
| Fe powder (#894186) | | 27.0 | 31.0 | | | |
| 0 | 0.29193 | 17.4 | 29.7 | 170 | 199.0 | –33 |
| 5 | 0.29101 | 99.6 | 21.6 | 159 | 167.2 | –35 |
| 10 | 0.29079 | 13.6 | 10.2 | 152 | 71.6 | –42 |
| 15 | 0.29032 | 61.4 | 12.0 | 135 | 159.2 | –74 |
| 20 | 0.29011 | 19.0 | 20.2 | 127 | 163.2 | –45 |
| 25 | 0.29002 | 28.0 | 20.3 | 97 | 318.4 | –23 |

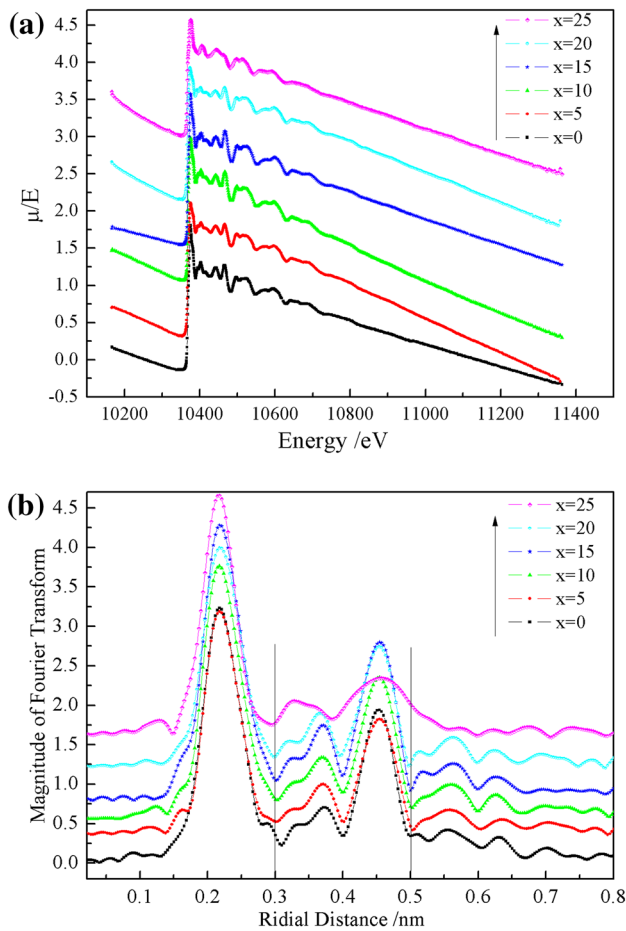


Fig. 3 EXAFS GaK-edge spectra (a) and its Fourier transforms (b) of the ribbons

concentration $x \leq 10$ retain A2 single phase, implying that Ga and Ni atoms substituted Fe atoms randomly. For ribbons with $x=15$ and $x=20$, they maintain A2 matrix despite a little amount of ordered phase emerge such as B2 and E2₁ phase. Although the ordered phases were detected in HRXRD patterns and micrograph, no obvious change was observed in the result of EXAFS. The size of precipitated phase is so small as to have no obvious influence on the EXAFS. Cao et al. [30] used neutron diffuse scattering to study the Fe–Ga alloys and detected precipitates with small size which have a large elastic strain. From this viewpoint, they concluded an evidence of structural origin for the enhanced magnetostriction [30]. For ribbon with Ni concentration $x=25$, one part of bcc phase transform into fcc phase and the phase structure in the ribbon is A2 and L1₂ phase. In other words, all studied ribbons are bcc matrix except the sample with $x=25$.

The magnetization curves are shown in Fig. 4a. The values of M_s and H_s are listed in Table 1. As the Ni concentration x increased, M_s decreased from 170 emu/g for $x=0$ to 97 emu/g for $x=25$. The reason of M_s decrease is

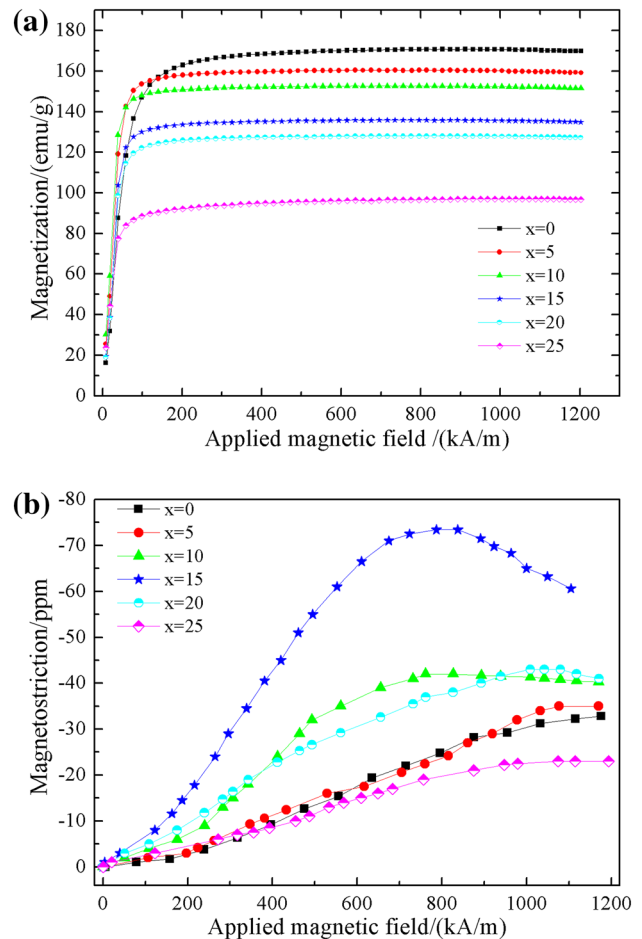


Fig. 4 a The magnetization curve of the sample. The direction of the applied magnetic field was parallel to the direction of the band length. b The magnetostrictive coefficient curve of the sample, the strain gauge stuck along the strip length direction, and the magnetic field was perpendicular to the strip surface

mainly that the magnetic moment of Ni atom is smaller than that of Fe atom. It is worth mentioning that the value of M_s decreases slowly when $x \leq 10$ but there are two drastic change at $x=15$ and $x=25$. We believe that it can be explained with structural transformation. The B₂ phase and L1₂ phase have a lower saturation magnetization than that of A₂ phase, so the value of M_s exhibit an obvious decrease at $x=15$ due to the emergence of ordered phase [31]. As for the ribbon with $x=25$, the dramatic decrease of M_s implies an obvious change in structure. This structural change is also confirmed by the result of EXAFS and micrograph just as described in the former part of this paper. The saturation magnetic field H_s is 199.0 kA/m for Fe₈₁Ga₁₉ ribbon without Ni doping. Continuing substitution of Ni for Fe in FeNiGa ribbons reduced H_s . H_s reached the minimum value of 71.6 kA/m for $x=10$. When the Ni concentration x was larger than 10, H_s increased and reached the maximum value of 318.4 kA/m for ribbon with $x=25$.

The magnetostrictive coefficient curves of FeNiGa ribbons are shown in Fig. 4b. The results show that the saturated magnetostriction coefficient of the sample increases gradually with the increase of Ni content x , from -33 ppm at $x=0$ to -74 ppm at $x=15$. With the increase of x , the value of λ_s decreases gradually until it reaches the minimum of -23 ppm at $x=25$. The specific values of magnetostriction coefficient are shown in Table 1.

From Table 1 we got the variation of I_{200}/I_{110} ratio, λ_s and H_s with the change of Ni composition for FeNiGa ribbons. The variation curve is shown in Fig. 5. The change of H_s with (110) texture can be explained as follows: for Fe–Ga-based alloys, [100] orientation is the easy axis while [110] orientation is the hard one [32]. The prefer orientation is along the normal direction of ribbons due to the temperature gradient. Thus [110] orientation is along the ribbon normal direction and the easy axis is along the ribbon length direction. Therefore, when the magnetic field is applied along the ribbon length direction, the stronger (110) texture, the smaller magnetic field is needed for the ribbons to be saturated. Comparing the variation of H_s and λ_s we observe that the change of H_s is almost contrary to λ_s . This means that the ribbon will be of large magnetostriction if it is easy to saturate along the ribbon length direction. It is well known that the magnetic materials consist of magnetic domains which are separated by domain wall. When the magnetic field is applied upon the magnetic materials, magnetic domains rotate to the orientation of magnetic field

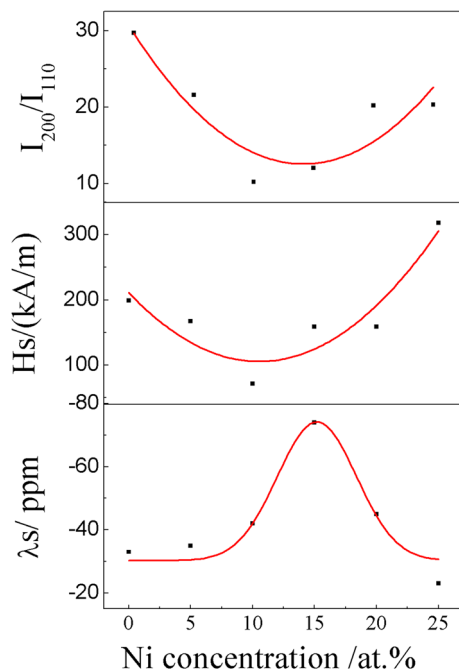


Fig. 5 The variation curve of I_{200}/I_{110} , H_s and λ_s with Ni concentration x

until saturation. According to this viewpoint, the easier to saturate along 0° orientation the material is, the harder to saturate along the 90° orientation. Back to our discussion, in ribbon with Ni concentration $x=15$, it exhibits the strongest (110) texture, which makes the ribbon easier to saturate in magnetization along ribbon length direction, implying it is most difficult to saturate along the normal direction of ribbon. This means when the magnetic field is applied along the ribbon normal direction, there will have more magnetic domains to rotate. The rotation of magnetic domains results in an increase of magnetoelastic energy and then induces large magnetostriction [33]. Hence we obtained largest magnetostriction in ribbon with $x=15$ when the magnetic field was applied along the ribbon normal direction. From above, we summarize the relation among (110) texture, H_s and λ_s . That is, the strongest (110) texture creates the lowest H_s and the highest λ_s .

In general, the doping of Co, Ni and other elements will stabilize DO_3 in Fe–Ga based alloys, which will lead to the decrease of magnetostrictive properties [20]. However, the existence of DO_3 phase has not been detected in this paper. With the gradual substitution of Ni for Fe, the magnetostrictive coefficient shows an increasing trend. In Fe–Ga binary alloys, the large magnetostrictive coefficient is considered to be related to modified- DO_3 phase. Another expression is that the next-nearest-neighbor pairs of Ga–Ga atoms are arranged along the direction of [100], and the effect of (100) texture should also be taken into account [4]. However, no modified- DO_3 phase and (100) texture were found in the reported FeNiGa alloys, so there are other factors affecting the magnetostrictive properties of FeNiGa alloys. The analysis shows that the (110) texture in FeNiGa alloy leads to the decrease of H and the increase of λ_s . Therefore, it can be considered that (110) texture can promote the magnetostrictive properties of FeNiGa alloy. In addition, the effect of phase structure must be taken into account, because other ordered phases besides A2 phase have been found in the samples studied. When $x < 10$, the sample is A2 single-phase structure, and the magnetostriction coefficient is low. $L1_2$ phase is considered to inhibit the magnetostrictive properties of Fe–Ga alloys [34–36]. By comparing and studying the phase structure of the samples, it can be concluded that besides the effect of texture, a small amount of $E2_1$ in the sample $x=15$ is beneficial to the magnetostrictive properties of FeNiGa alloy.

4 Conclusions

The effect of Ni doping on the structure and magnetic properties of Fe–Ga ribbons has been studied. When $x < 10$, the ribbon was A2 single-phase structure; when $x=15$ and $x=20$, the ribbon maintained the main structure of A2 phase

except for partial ordered phase; When $x=25$, the partial bcc structure of the ribbon transformed into fcc structure. As the content of Ni increased, Ms decreased because smaller magnetic moment of Ni. Meanwhile, Hs decreased first and then increased, and reached its minimum at $x=10$. At the same time, with the formation of the main structure of $L1_2$ phase, part of $E2_1$ phase precipitated. At $x=15$, the saturation magnetostriction coefficient of the sample reached the peak value of -74 ppm. $E2_1$ phase promoted the magnetostrictive properties of FeNiGa ribbons. In addition, the strength of (110) texture showed the same trend with the change of magnetostrictive properties of samples as shown in Fig. 5. In samples with stronger (100) texture, the increase of magnetoelastic properties caused by domain rotation led to the improvement of magnetostrictive properties. Thus (110) texture was considered to be beneficial to the magnetostrictive properties of FeNiGa. Our work provides practical insights into magnetostriction of transition metal doped Fe–Ga alloys, which will guide the design of new, low-cost, giant magnetostrictive materials.

Acknowledgements We acknowledge the beam lines BL14B and BL14 W of Shanghai Synchrotron Radiation Facility (SSRF) for the provision of beam time. The study was supported by National Natural Science Foundation of China (Grant Nos. U1832143, 11604067, 51805048) and the Natural Science Foundation of the Jiangsu Higher Education Institutions of China (No. 18KJD140005).

References

1. M. Wuttig, L. Dai, J. Cullen, Elasticity and magnetoelasticity of Fe–Ga solid solutions. *Appl. Phys. Lett.* **80**, 1135 (2002)
2. A.E. Clark, K.B. Hathaway, M. Wun-Fogle, J.B. Restorff, T.A. Lograsso, V.M. Keppens, G. Petculescu, R.A. Taylor, Extraordinary magnetoelasticity and lattice softening in bcc Fe–Ga alloys. *J. Appl. Phys.* **93**, 8621 (2003)
3. N. Srisukhumbowornchai, S. Guruswamy, Large magnetostriction in directionally solidified FeGa and FeGaAl alloys. *J. Appl. Phys.* **90**, 5680 (2001)
4. T.A. Lograsso, A.R. Ross, D.L. Schlagel, A.E. Clark, M. Wun-Fogle, Structural transformations in quenched Fe–Ga alloys. *J. Alloys Compd.* **350**, 95 (2003)
5. C.J. Quinn, P.J. Grundy, N.J. Mellors, The structural and magnetic properties of rapidly solidified Fe $_{100-x}$ Ga $_x$ alloys, for $12.8 \leq x \leq 27.5$. *J. Magn. Magn. Mater.* **361**, 74 (2014)
6. J. Zhang, T. Ma, M. Yan, Effect of heat treatment on structure, magnetization and magnetostriction of Fe $_{81}$ Ga $_{19}$ melt-spun ribbons. *Physica B* **404**, 4155 (2009)
7. R. Wu, Origin of large magnetostriction in FeGa alloys. *J. Appl. Phys.* **91**, 7358 (2002)
8. J. Cullen, P. Zhao, M. Wuttig, Anisotropy of crystalline ferromagnets with defects. *J. Appl. Phys.* **101**, 123922 (2007)
9. Y. He, X. Ke, C. Jiang, N. Miao, H. Wang, J.M.D. Coey, Y. Wang, H. Xu, Interaction of trace rare-earth dopants and nanoheterogeneities induces giant magnetostriction in Fe–Ga alloys. *Adv. Funct. Mater.* **28**, 1800858 (2018)
10. R. Wu, Z. Yang, J. Hong, First-principles determination of magnetic properties. *J. Phys.: Condens. Matter* **15**, S587 (2003)
11. C. Bormio-Nunes, R.S. Turtelli, R. Grössinger, H. Müller, H. Sassik, Magnetostriction of melt-spun Fe $_{85}$ Ga $_{15}$, Fe $_{78}$ Ni $_{7}$ Ga $_{15}$ and Fe $_{78}$ Co $_{7}$ Ga $_{15}$ stacked ribbon samples. *J. Magn. Magn. Mater.* **322**, 1605 (2010)
12. A.E. Clark, in *Magnetostrictive Rare Earth-Fe $_2$ Compounds*, ed. by E.P. Wohlfarth (North-Holland publishing Company, Amsterdam, 1980), p. 531
13. L. Jiang, J. Yang, H. Hao, G. Zhang, S. Wu, Y. Chen, O. Obi, T. Fitchorov, V.G. Harris, Giant enhancement in the magnetostrictive effect of FeGa alloys doped with low levels of terbium. *Appl. Phys. Lett.* **102**, 222409 (2013)
14. Y. Han, H. Wang, T. Zhang, Y. He, C. Jiang, Exploring structural origin of the enhanced magnetostriction in Tb-doped Fe $_{83}$ Ga $_{17}$ ribbons: tuning Tb solubility. *Scr. Mater.* **150**, 101 (2018)
15. Y. He, C. Jiang, W. Wu, B. Wang, H. Duan, H. Wang, T. Zhang, J. Wang, J. Liu, Z. Zhang, P. Stamenov, J.M.D. Coey, H. Xu, Giant heterogeneous magnetostriction in Fe–Ga alloys: effect of trace element doping. *Acta Mater.* **109**, 177 (2016)
16. W. Wu, C. Jiang, Improved magnetostriction of Fe $_{83}$ Ga $_{17}$ ribbons doped with Sm. *Rare Met.* **36**, 18 (2017)
17. Y. Liu, J. Li, X. Gao, Influence of intermediate annealing on abnormal Goss grain growth in the rolled columnar-grained Fe–Ga–Al alloys. *J. Magn. Magn. Mater.* **435**, 194 (2017)
18. R.C. Hall, Single-crystal magnetic anisotropy and magnetostriction studies in iron-base alloys. *J. Appl. Phys.* **31**, 1037 (1960)
19. A.E. Clark, J.B. Restorff, M. Wun-Fogle, K.B. Hathaway, T.A. Lograsso, M. Huang, E. Summers, Magnetostriction of ternary Fe–Ga–X (X=C, V, Cr, Mn Co, Rh) alloys. *J. Appl. Phys.* **101**, 09C507 (2007)
20. N. Kawamiya, K. Adachi, The magnetic properties of (Fe $_{1-x}$ Mx) $_3$ Ga. *J. Magn. Magn. Mater.* **31**, 145 (1983)
21. S. Fujieda, R. Ukai, Y. Onuki, S. Suzuki, Influence of Co substitution on magnetostriction and on Young's modulus of Fe–Ga alloy single crystal. *AIP Conf. Proc.* **1649**, 27 (2015)
22. S.F. Xu, H.P. Zhang, W.Q. Wang, S.H. Guo, W. Zhu, Y.H. Zhang, X.L. Wang, D.L. Zhao, J.L. Chen, G.H. Wu, Magnetostriction and electrical resistivity of Mn doped Fe $_{81}$ Ga $_{19}$ alloys. *J. Phys. D Appl. Phys.* **41**, 015002 (2008)
23. L. Dai, J. Cullen, M. Wuttig, T. Lograsso, E. Quandt, Magnetism, elasticity, and magnetostriction of FeCoGa alloys. *J. Appl. Phys.* **93**, 8627 (2003)
24. J.B. Restorff, M. Wun-Fogle, A.E. Clark, T.A. Lograsso, A.R. Ross, D.L. Schlagel, Magnetostriction of ternary Fe–Ga–X alloys (X= Ni, Mo, Sn, Al). *J. Appl. Phys.* **91**, 8225 (2002)
25. V. Raghavan, Fe–Ga–Ni (Iron-Gallium-Nickel). *J. Phase Equilib. Diffus.* **30**, 98 (2008)
26. T. Takahashi, K. Hashimoto, T. Okazaki, Y. Furuya, T. Kubota, C. Saito, Characterization of magnetostrictive Fe–Ga-based alloys fabricated by rapid solidification. *Scr. Mater.* **60**, 847 (2009)
27. Y. Ke, C. Jiang, J. Tao, H. Duan, Local inhomogeneous structural origin of giant magnetostriction in Fe–Ga alloys. *J. Alloys Compd.* **725**, 14 (2017)
28. S. Altin, E. Oz, E. Altin, S. Demirel, A. Bayri, S. Avci, Investigations of the capacity fading mechanism of Na $_{0.44}$ MnO $_2$ via ex situ XAS and magnetization measurements. *Dalton Trans.* **47**, 17102 (2018)
29. Á. Ravel, M. Newville, ATHENA, ARTEMIS, HEPHAESTUS: data analysis for X-ray absorption spectroscopy using IFFEFIT. *J. Synchrotron Radiat.* **12**, 537 (2005)
30. H. Cao, P. Gehring, C. Devreugd, J. Rodriguez-Rivera, J. Li, D. Viehland, Role of nanoscale precipitates on the enhanced magnetostriction of heat-treated galfenol (Fe $_{1-x}$ Ga $_x$) alloys. *Phys. Rev. Lett.* **102**, 127201 (2009)
31. N. Kawamiya, K. Adachi, Y. Nakamura, Magnetic properties and mössbauer investigations of Fe–Ga alloys. *J. Phys. Soc. Jpn.* **33**, 1318 (1972)

32. A. Kumagai, A. Fujita, K. Fukamichi, K. Oikawa, R. Kainuma, K. Ishida, Magnetocrystalline anisotropy and magnetostriction in ordered and disordered Fe–Ga single crystals. *J. Magn. Magn. Mater.* **272**, 2060 (2004)
33. F. Bai, H. Zhang, J. Li, D. Viehland, Magnetic force microscopy investigation of the static magnetic domain structure and domain rotation in Fe-x at.% Ga alloys. *Appl. Phys. Lett.* **95**, 152511 (2009)
34. H. Basumatary, M. Palit, J.A. Chelvane, D.A. Babu, R. Sarkar, S. Pandian, Microstructure and magnetostriction of melt-spun Fe₇₃Ga₂₇ ribbon. *Appl. Phys. Lett.* **101**, 144106 (2012)
35. Y. Du, M. Huang, S. Chang, D.L. Schlagel, T.A. Lograsso, R.J. McQueeney, Relation between Ga ordering and magnetostriction of Fe–Ga alloys studied by X-ray diffuse scattering. *Phys. Rev. B* **81**, 054432 (2010)
36. N. Srisukhumbowornchai, S. Guruswamy, Influence of ordering on the magnetostriction of Fe-27.5 at.% Ga alloys. *J. Appl. Phys.* **92**, 5371 (2002)

Publisher's Note Springer Nature remains neutral with regard to jurisdictional claims in published maps and institutional affiliations.